EUROPEAN FUSION DEVELOPMENT AGREEMENT

EFDA–JET–CP(01)07-2

V. Riccardo, P. Andrew, G. Maddaluno and JET EFDA Contributors

Disruption Heat Loads on the JET MkIIGB Divertor

Disruption Heat Loads on the JET MkIIGB Divertor

V. Riccardo[1], P. Andrew[1], G. Maddaluno[2]
and JET EFDA Contributors

[1]UKAEA/Euratom Fusion Association, Culham Science Centre, Abingdon OX14 3DB, UK
[2]ENEA/Euratom, Frascati, Viale E. Fermi 45, 00044 Frascati, Roma, Italy
** See the appendix of JET EFDA contributors (prepared by J. Paméla and E.R Solano),*
"Overview of JET Results",
Fusion Energy 2002 (Proc. 19th Int. Conf. Lyon, 2002), IAEA, Vienna (2002).

Preprint of Paper to be submitted for publication in Proceedings of the
IAEA Technical Committee Meeting on Divertor Concept,
(Aix-en-Provence, France 11-14 September 2002)

ABSTRACT

Disruption heat loads are one of the major concerns for the safe and reliable operation of plasma facing components. Understanding how the plasma energy is distributed during the disruption could help in developing design criteria.

Although the stored energy of the JET plasmas is small compared to that foreseen for the next generation tokamaks, analysis of JET disruptions could still provide valuable information on the distribution of the energy loads.

Combined analysis of divertor thermocouple and infrared camera measurements can provide some insight on the disruption heat load distribution.

When the energy quench occurs at the same time as, or after, the loss of plasma vertical control, no significant divertor tile temperature increase can be observed for upwards (away from the divertor) events. When the plasma energy is lost with the plasma still in X-point configuration, the septum and the tiles wetted by the strike-points, often more than one tile per strike-point, experience a sharp increase in temperature, equivalent to up to 1MJ/m^2, much larger than those experienced in faster quenches.

Most of the disruptions purposely made to produce run-away electrons went towards the divertor and, although not systematically, lead to local (mostly at the septum) temperature increase equivalent to a load up to 2MJ/m^2, often toroidally asymmetric.

1. INTRODUCTION

The divertor thermocouples (TCs) and the infra-red (IR) view of the divertor can be used to estimate the amount and distribution of energy deposited during disruption. Unfortunately, the bolometry is not reliable in disruption, therefore the full energy balance cannot be checked.

The aim of this analysis is to provide an estimate of the energy density deposited on the divertor during disruptive events. In section 2 the experimental set up (divertor geometry and material properties, and the available diagnostics) is given. In section 3 first a few disruptions are analyzed in detail, then the sets of recent deliberate disruptions are discussed. In particular for the disruption mitigation experiments links between evidence of plasma/divertor interaction and halo-related loads are investigated. A tentative discussion of the global energy balance, including the magnetic component, is given in section 4. Finally section 5 draws some conclusions out of the results presented.

2. THE MKIIGB DIVERTOR AND ITS DISRUPTION RELEVANT DIAGNOSTICS

The JET MkIIGB divertor is divided into 24 modules (Fig.1). In each module the tiles and the carriers are made of CFC (Carbon Fiber Composite). In most of the target tiles the weave lies on the (θ, $\perp$)-plane while in the vertical target tiles it is on the (ϕ, $\perp$)-plane (Fig.1). One of the directions of good conductivity is dictated by the need to promptly remove the heat from the surface subject to the plasma load. The other direction has been imposed by mechanical strength and manufacturing constraints (e.g. size, shape, accuracy). The thermal properties of the tile material have been measured on samples taken from the MkIIa and the MkIIGB batches and are shown in Fig. 2; the average tile density is 1820kg/m^3.

The divertor is observed by an IR camera (Fig. 3), which detects photons in the 3.5-5μm region. The detector collects data on four 2D sub-arrays (64x64 pixels each) at arate of ~20μs/lines. The endoscope is located at the upper limiter guide tube of octant 4 (about 25cm above the midplane). The field of view is split into two tangential views of the inner and outer divertor, so that both strike-points are visible in most plasma configurations.

Embedded in the JET MkIIGB target tiles are ~40 TCs. These are fitted ~10mm below the plasma facing surface and are evenly distributed poloidally as shown in Fig.4. This provides a reasonable poloidal profile of the disruption energy distribution on the divertor [1,2].
Figure 4 also includes the magnetic diagnostics present in the divertor:

- eleven 2D poloidal field pick-up coils are fitted in the divertor support structure,
- one halo probe (a toroidal field pick-up coil) is located at the divertor base above the structure and
- two poloidal current shunts are present in the divertor support structure (not shown in Fig.4).

The plasma current and position is calculated during disruption, as well as in the rest of the discharge, using two sets of 18 poloidal field pick-up coils and 14 saddle loops. These magnetic diagnostics, together with the coils near along the poloidal limiter trace are used to reconstruct the plasma shape; however, often in disruptions the plasma shape cannot be obtained in this way. The information form the magnetic diagnostics can be complemented with that of the Soft X-Ray (SXR) cameras, which are especially valuable in the analysis of events leading to the generation of runaway electrons (RE) as to determine the location and intensity of the beam. RE events are identified by their characteristic signature on the hard X-Ray (HRX) camera. In addition, there is often a plateau during the plasma current decay.

Unfortunately the JET bolometry cannot be trusted during disruptions: excessive heating of the detectors translates in an overestimate of the total radiated energy (the energy calculated from the bolometers systematically exceeds the pre-disruption plasma stored energy). The lack of a reliable measure of the radiated energy leads to substantial uncertainties in the disruption energy balance.

3. DIVERTOR HEAT LOADS AS MEASURED BY THERMOCOUPLES AND INFRA-RED CAMERA

The analysis of the thermocouple signals after upward (i.e. away from the divertor) disruptions of low energy plasmas indicates that these are subject to an error due to poloidal field pick-up by stray loops in the region where the wiring is located. The error depends on the plasma current and the quench time, and it can be as large as 30C, which in most cases is comparable with the temperature increase that has to be measured.

In order to determine the actual temperature increase it is necessary to consider the long-term evolution of the signal, and to decrease the relative error high stored energy plasmas are preferable for this analysis. However, the disruptions most suitable for TC analysis are those of plasma configurations with non-disruptive references. In the following, four of these cases will be presented and discussed.

The tile temperature increase has been also reproduced using 2D finite element (FE) models, to

estimate the amount of energy deposited on each tile, which is summarized in Table 1 for the four cases analyzed in the following subsection.

The 2D FE models have been benchmarked by reproducing both TC and IR measurements. An example is reported in Fig.5 for Pulse No: 54287, a deliberate downward disruption during which the sides of the septum tile have been touched by the strike-points. The same FE model has been run to reproduce both the TCs alone and the TCs together with the IR measurements, using different boundary conditions.

Although the method to reproduce both IR and TC will not be full exploited in the following (IR data are not always available), this is the most interesting of the two approaches. In fact, this does not only give the deposited energy density, but it provides also an estimate of the film heat transfer coefficient which needs to be assumed if the temperature observed by the IR has to be reproduced. The presence of the layer is not just a numerical trick, it has been observed both on MkIIa and on MkIIGB [3]. In the case of Pulse 54287, the heat transfer coefficient, which fits best at the septum tile, is 10kW/(m^2K) and the applied energy density to obtain the TC readings is 0.2MJ/m^2. Most of the uncertainty in the estimate of the total energy deposited on to the septum row of tiles lies in the wetted area. Both from the IR image and from the similarity between the septum inboard and outboard TC temperatures (Fig.5a), it can be assumed that roughly the same amount of energy was deposited on both sides of the tile. In addition from the IR image, the size of the footprint seems to be ~0.040.02m, so the total deposited energy is 0.060.19MJ.

3.1 ANALYSIS OF SINGLE DISRUPTIONS

Pulse 51976 had the strike-points on the inner vertical and the outer horizontal tiles. It disrupted losing its energy and current in about 20 ms. Comparison of the TC traces for Pulse No: 51976 with those of Pulse No: 51972 (identical up to the disruption) shows that the strike-points move up to the baffle tiles (Fig.6). In fact, the temperature of the tiles at the initial strike-point position increases more slowly than in the non-disruptive reference, or even reverses, while the temperature of the baffle tiles increases substantially. It is worth noting that both the outer baffle TCs register a temperature increase, as if the heat load had been spread on a rather large portion of the tile surface. Also the IR, Fig.7, measures an increase (up to 800^{o}C) of the outer baffle tile temperature (which can be consistent with the TC data), but the most evident impact of the disruption appear at the inner vertical tile (a fast growing and fast decaying temperature variation, up to 1500^{o}C). The enhanced rate of change of the temperature could be attributed to a loosely attached surface layer, which both heats up and cools down much faster than clean surfaces. The effects of this layer are typically observed during ELMs and they are the stronger the closer the location of the interaction is to the inner louver, the coldest place in the divertor where most of the co-deposited hydrogen isotopes have been found following the D-T campaign [3].

Pulse No: 51989 was a disruptive repeat of pulse 51988 (Fig.8). At the time of the NBI heating, the strike-points were on the vertical tiles. Apart from a slight decrease in temperature at the strike-point tiles after the disruption, the only major difference between the TC time traces of these two shots is in the large temperature increase at the septum. This is a rather typical outcome of disruptive events.

A non-disruptive reference for Pulse No: 52018 is 52021 (Fig.9). Also in this case there is a substantial temperature increase at the septum, but other features appear too. The outer horizontal and the inner vertical and horizontal tiles become hotter. Although the temperature at the baffle tiles stays below that of the reference pulse, as these are wetted by the tail of the power deposition profile, its time derivative just after the energy quench is higher, as if transiently their thermal load has been higher too. Such a broad distribution of energy could indicate that the strike-points swept over a large poloidal arc during the energy quench, which in this case starts almost half a second before the loss vertical stability and the current quench and occurs very slowly (Fig.10). Alternatively, the SOL footprint on the divertor has expanded. In either case, up to two thirds of the pre-disruption plasma stored energy have been distributed rather uniformly on a large area of the divertor.

Both Pulse No: 53790 and 54327 (Fig.11) are deliberate disruptions (achieved by puffing Argon) of outer poloidal limiter configurations, that produced RE and went towards the divertor (downwards). However, only the latter seems to have interacted with the septum in the vicinity of the toroidal location of the TCs, leading to $>40^{o}$C increase in temperature. While in most of the disruptions the energy associated with the measured tile temperature variations assuming toroidal symmetry is well below the pre-disruption plasma stored energy (Table 1), in the case of some RE disruptions it is close (as for 54327) or even exceeds this. In addition, generally the septum temperature tends to vary in a toroidally symmetric way (e.g. 52018 in Fig.12a), but in some RE events (e.g. 54327 in Fig. 12b and in some of those listed in Table 2 and 3) the symmetry seems to have been broken. An uneven heat load distribution could reconcile the deposited with the pre-disruption stored energy for the RE disruption discussed above.

This could also explain why very similar disruptive events (e.g. 53790 and 54327) lead to such differences in the TC measurements: in the case of pulse 53790 most of the RE beam missed the toroidal locations of the TCs. An alternative explanation for the TC overestimate of the divertor deposited energy could have been the volumetric heating of the RE beam. At the energy levels typical for JET RE (10-20MeV) up to 1cm perpendicular to the beam direction can be penetrated. However, the incidence angle is so shallow ($<4^{o}$) that the RE volumetric heating can be approximated with a surface load without significant errors in the temperature variation observed by the TCs.

3.2 ANALYSIS OF C1-C4 DELIBERATE DISRUPTIONS

Two areas were covered by the disruption studies during last year operation: RE and disruption mitigation (using fast He puffing).

The plasma configuration chosen for the RE experiments (Table 3 and 4) has low elongation and it is limited by the outer poloidal limiter. This has been selected as it produced the best RE events in spontaneous disruptions (Table 2). This kind of configuration has the additional advantage (from the point of view of divertor disruption heat load analysis) of keeping the divertor uniformly cold until the time of the event. The IR is the diagnostic which can take maximum benefit from the above characteristic of the RE disruptions. In fact, counting the number of frames with significant light recorded by the IR camera is possible to obtain a reasonable estimate of the duration and the location of the plasma/divertor interaction, without the interference due to the presence of previously

heated regions. As expected from the analysis of the response of the inner and outer targets to ELM, the presence of a weak thermal connection between the surface layer and the bulk of the tile seems evident at the inner horizontal and vertical tiles. Once short temperature spikes at the inner target have been neglected, the poloidal patterns observed by the TC and the IR are in reasonable agreement, especially if possible toroidal asymmetries are included in the analysis. In fact, in most of the RE disruptions (differently from other disruptions) there is a difference of up to 50% between the temperature increase of the septum in two different toroidal locations (modules 4 and 9, which are 75^{o} apart). Overall there seem to be a good correlation between HXR, SXR (indicating the presence of RE) and divertor temperature increase. In addition, in the RE-prevention disruptions the beneficial effect of Helium puffing on the outcome of the disruption are seen both in the lack of RE signatures and in a smaller heat load on the divertor (Table 4). Two configurations have been used in the vertical disruption event (VDE) amelioration experiments. These are a low-triangularity medium-elongation 2 MA/2.6 T and a ITER-like shape 1.5MA/1.6T. The VDE-amelioration test discharges (Table 5) were run ohmically at rather low plasma current and no substantial temperature variation has been measured by the divertor TCs. The IR shows some increase in the divertor temperature only in downward events. In these cases the septum surface seems to have heated up to a temperature compatible with the measured temperature increase in the bulk of the tile only if the weakly attached surface layer is accounted for. Considering the only two deliberate downward disruptions with the IR available (54287 with Helium puffing and 54288 without Helium puffing), it seems that the injection of Helium does not decrease the divertor heat loads in X-point configurations (while it does in limiter configurations, see above). In fact, the septum surface temperature rises to 500^{o}C in 54287 and to 350^{o}C in 54288. Most likely this is due to a longer interaction between the plasma and the divertor, as the main effect of Helium puffing is to extend the duration of the current quench. In addition, this disruption mitigation technique had some success at decreasing the peak of the poloidal halo current (in Fig. 13 there are the measurements from the toroidal pick-up coil, a similar conclusion can be drawn from the poloidal current shunts). However, it failed in substantially reducing the disruption vertical force on the vessel. On the contrary, the vessel reaction was larger after disruptions with Helium puffing than after those without it, see the vertical vessel force (Fv), and the vessel sideways displacement (RSide) columns in Table 5. This again can be explained by the extended duration of the current quench, in fact the force impulse on the vacuum vessel, somewhat proportional to the time integral of the variation of vertical current moment, is larger (Fig.13).

4. ENERGY BALANCE

The energy balance during disruptions in JET is difficult to check as this is not well diagnosed. The JET bolometry is affected by excessive heating of the detectors. An accurate space and time integral of the divertor loads cannot be carried out with the present TC and IR diagnostics. Experience in other tokamaks shows that most of the energy of an ohmic plasma [4] is radiated during disruption, and that most of the plasma thermal energy during the energy quench and about 30% of the ohmic energy during the current quench [5] is deposited onto the divertor. At least qualitatively the observed divertor deposited energy at JET seems to be in line with the experience in other tokamaks. In fact,

when the energy quench occurs after the loss of the X-point, like in pulses 51976 and 51989 in Table 1, only a modest fraction of the pre-disruption stored energy is deposited on to the divertor. Instead when the plasma loses its energy whilst still in diverted configuration, like in pulse 52018 in Table 1, up to two thirds of the pre-disruption stored energy land on the divertor.

Unfortunately the only quantitative check that can be performed is the one on the small exchange of energy between the plasma and the poloidal field coils. Using the JET self and mutual inductance of the poloidal field coil system, the vacuum vessel shell and the plasma together with the measured coil and plasma current and position it is possible to determine the ohmic dissipation during a disruption. As a sample case Pulse No; 51976 is reported. During the current quench the plasma equivalent self inductance, which includes also the plasma kinetic energy, can be expressed as

$$L_p = \mu_0 R \left(\ln \frac{8R}{4} - 2 + \frac{l_i}{2} + \frac{3}{4} \beta_p \right).$$

The plasma self inductance is kept constant to 10 μH during the disruption, as this is an acceptable approximation of its actual variation.

The vessel has been represented by nine toroidal shells with an equivalent self inductance, mutual inductance and resistance in order to compute the induced currents.
For each toroidal component the self-magnetic energy has been calculated as

$$\Delta W_i^L = \int I_i \frac{d}{dt} (L_i I_i) dt,$$

the mutual-magnetic energy as

$$\Delta W_i^M = \sum_{i \neq j} \int I_i \frac{d}{dt} (M_{ij} I_j) dt,$$

and the ohmic heating energy as

$$\Delta W_i^{\Omega} = \int R_i^2 I_i \, dt,$$

The net loss of plasma energy (Fig. 14), equal to the variation of the sum of the plasma self and mutual magnetic energy, is comparable with the pre-disruption plasma stored energy (10 MJ). The external (poloidal field coils and vacuum vessel) magnetic energy does not vary substantially during the disruption (Fig.14). This indicates that the amount of energy lost through the magnetic channel and transferred to the external toroidal components is small.

CONCLUSIONS

The poloidal distribution of the energy deposition observed in disruptions with high thermal plasma energy seems to indicate that of the zone of interaction between the plasma and the divertor either broadens or sweeps during the energy quench. This has a beneficial effect on the average energy

density, which in symmetric events has not been found above 1MJ/m^2. The highest energy density was recorded in a slow (~500ms) disruption starting with 5MJ plasma stored energy. If a similar event happened at the stored energy level typical for ITER (>500MJ), on a divertor with twice the JET characteristic dimension and with a similar footprint width, this would lead to an energy density ~50MJ/m^2, which is in line with the present ITER assumptions [6]. No substantial toroidal asymmetry in the divertor energy deposition has been recorded in events other than those with RE. This is encouraging as it minimizes the peak heat load.

The fast Helium-puffing RE-prevention experiments performed on outer poloidal limiter limited configurations proved successful in eliminating both the RE beam and in avoiding any substantial interaction between the disrupting plasma and the divertor. Less clear is the result of the VDE mitigation experiments, also achieved by puffing Helium at high (up to 2400 mbarl) rate. The main effect of the Helium puff was to slow down the current quench, as if the additional gas formed a barrier around the plasma, protecting it from the influx of impurity due to the plasma/wall interaction. The lengthened event resulted in higher heat loads (at least in the few disruptions where the IR was available) and vessel reactions (vertical force and sideways displacement). The lack of efficiency in ameliorating the disruption might be due to the small amount of gas that could be injected with the present system: the plasma just behaved as in a Helium plasma density limit. On the contrary in recent Asdex Up Grade experiments [7], where a lar ger ratio of Helium to plasma particles could be injected, at least the current quench speed actually increased.

As the JET bolomentry is affected by over-heating during disruption, neither the time dependent power nor the global energy balance could be checked for the set of disruptions discussed above. Analysis of the IR data was limited. This is partly because reliable measurements have been obtained only for recent shot, and partly because of the modeling complications necessary to account for the effects of high power density on the weakly connected (thermally) surface layer. In order to be properly simulated this layer requires different heat transfer coefficients along the poloidal angle and maybe also depending on the actual conditioning of the tile. Only the total energy deposited on to the divertor could be estimated by using the TCs, but this with a rather large error bar, due to the uncertainty on the contact region between the plasma and the tiles. Therefore the only clear observation is that generally the thermal load during the energy quench (which constitutes the largest disruptive contribution) is distributed over more that one tile (~200 mm each) at each strike-point.

ACKNOWLEDGEMENTS

This work has been conducted under the European Fusion Development Agreement and is partly funded by Euratom and the UK Department of Trade and Industry. The authors would like to thank C. Ingesson (for his help in understanding the problems with the JET bolometry), E. Solano (for the queries on magnetic energy interchange with the external systems) and T. Eich (for the interface with the IR data).

REFERENCES

[1]. A.C. Janos et al., Disruptions in the TFTR tokamak, IAEA-CN-56/A-7-15 (1993) 527-539

[2]. M. Ciotti et al., Energy deposition on the FTU poloidal limiter during disruptions, Journal of Nuclear Materials, 220-222 (1995) 567-570

[3]. J.P. Coad et al., Erosion/deposition issues at JET, Journal of Nuclear Materials 290-293 (2001) **224-230**

[4]. K. Yamazani, G.L. Schmidt, Dissipation of magnetic energy during disruptive current termination, Nuclear Fusion **24** (1984) 467-472

[5]. G. Pautasso et al., Energy balance during disruption associated with vertical displacement events, Nuclear Fusion **34** (1994) 455-458

[6]. H. Wurst et al., Vertical target and FW erosion during off-normal events and impurity production and transport during ELMs typical for ITER-FEAT, Journal of Nuclear Materials **290-293** (2001) 1138-1143

[7]. G. Pautasso, private communication

Pulse No:	Plasma current [MA]	ΔE (MJ) inner baffle	ΔE (MJ) inner vertical	ΔE (MJ) inner horizontal	ΔE (MJ) septum	ΔE (MJ) outer horizontal	ΔE (MJ) outer vertical	ΔE (MJ) outer baffle	Divertor TC Energy [MJ]	Plasma stored Energy [MJ]
51976	2.5	0.1 ÷ 0.3	~0	~0	0.05 ÷ 0.15	~0	~0	0.2 ÷ 0.6	0.35 ÷ 1.05	10.
51989	1.5	~0	~0	~0	0.15 ÷ 0.45	~0	~0	~0	0.15 ÷ 0.45	2.3
52018	1.7	0.1 ÷ 0.3	0.1 ÷ 0.3	0.1 ÷ 0.3	0.3 ÷ 1.0	0.2 ÷ 0.6	~0	0.3 ÷ 0.9	1.1 ÷ 3.3	~5.
54327	2.0	~0	~0	~0	0.3 ÷ 0.9	~0	~0	0.06 ÷ 0.18	0.36 ÷ 1.08	1.3

Table 1: Estimate of the energy deposited on the divertor tiles (calculated from the thermocouple measurements with 2D FE models) and the pre-disruption plasma stored energy.

Pulse No:	Note	I_P (MA)	B_T (T)	Int (HXR)	TC	Comments
50219	Ip ramp-up	1.6	3.0	1.57	Septum only	40°C in module 4 & 15°C in module 9 (asymmetric)
51256	Ip ramp-up	1.0	3.0	3.18	Nothing	
51284	Ip ramp-up	1.6	3.0	2.28	Septum only	45°C in module 4 & 30°C in module 9 (asymmetric)
51328	Ramp down	1.4	3.3	3.57	Septum and outer baffle (10°C)	20°C in module 4 & 15°C in module 9 (almost asymmetric)
51506	Ip ramp-up	1.1	3.1	2.24	Nothing	

Tab20007

Table 2: Divertor heat loads of spontaneous disruptions leading to RE formation. No SXR or IR data are available for these disruptions. Also the pre-disruption plasma stored energy is not available. Only for the septum the axis-symmetry can be analyzed with some confidence. Int(HXR) is the time integral, over the current quench, of the HXR signal; this is in arbitrary, but pulse independent, units.

Pulse No:	I_p [MA]	B_T [T]	Int(HXR)	Ip-ind	E_p [MJ]	SXR [W/m^2]	TC	IR
53784	1.0	3.0	N/A	N/A	0.5	150	Nothing	N/A
53785	1.5	3.0	1.77	Y	1.0	500	20°C septum only (symmetric)	4 frames, mostly light
53786	2.0	3.0	4.38	Y	1.3	4000	<10°C inner baffle only	4 frames, inner hor. 400°C (fast light)
53787	2.5	3.0	0.8	?	1.7	400	septum (m4 25°C, m9 10°C)	10 frames, inner hor. 500°C, septum 500°C
53788	2.5	3.0	No	?	1.7	No	<5°C inner baffle only	12 frames, inner hor. 400°C, septum 350°C
53790	2.0	3.0	1.16	Y	1.3	5000	<5°C inner baffle, 10°C septum	4 frames, inner hor. 500°C, septum 200°C
53792	2.0	2.5	No	?	1.2	No	Nothing	2 frames, light spike only
53793	1.75	3.0	1.52	Y	1.1	600	<5°C inner baffle, 5°C septum	4 frames, inner hor. 300°C, septum 220°C
53794	2.25	3.0	2.6	Y	1.5	200	septum (m4 50°C, m9 15°C), 10°C outer baffle	5+3 frames, inner hor. 500°C, septum 400°C, (late) outer baffle 200°C
53795	1.5	2.5	No	?	0.8	40	Nothing	
53796	1.25	2.5	N/A	N/A	0.6	400	Nothing	N/A
54323	2.5	3.4	1.23	Y	1.8	4000	septum (m4 55°C, m9 15°C)	N/A
54325	2.0	3.4	2.63	Y	1.5	2500	5°C inner baffle only	N/A
54326	1.5	3.4	1.48	Y	1.2	1800	10°C inner baffle only	N/A
54327	2.0	3.0	2.07	Y	1.3	3500	septum (m4 45°C, m9 25°C)	N/A

Tab30107

Table 3: Divertor heat loads of deliberate (by Argon puffing) disruptions of outer poloidal limiter configurations leading to RE formation. When available, the IR has a sampling rate of ~2ms/frame and a default minimum temperature of 80° C in these discharges. Int(HXR) is the time integral, over the current quench, of the HXR signal; this is in arbitrary, but pulse independent, units. Ip-ind refers to the presence of a plateau during the plasma current decay. Ep is the pre-disruption plasma stored energy.

Pulse No:	Add. Gases	Int(HXR)	Ip-ind	SXR [W/m^2]	TC	IR	
54047	Ar	2.06	Y	2500	10^{0}C septum (symmetric)	Inner hor. and vert. 250^{0}C (1f), septum and outer baffle 20^0 (+f) IR rate: 17 ms/frame	
54048	Ar + He 1000 mbarl	No	?	35	Nothing	N/A	
54049	Ar + He 2400 mbarl	No	?	No	Nothing	Inner hor and vert, outer vert and baffle, septum 150^{0}C (10f) IR rate: 7 ms/frame	
54050	Ar	2.13	Y	4000	Septum (m4 15^{0}C and m9 10^{0}C), inner and outer baffle 5^{0}C	Inner hor and vert light only, outer vert and baffle 200^{0}C (6f), septum 250^{0}C (6f) IR rate: 7 ms/frame	
54279	Ar + He 230 mbarl	No	?	No	Nothing	Nothing	*Upwards*
54280	Ar + He 1000 mbarl	No	?	No	Nothing	Nothing	*Upwards*

Tab040107

Table 4: Divertor heat loads of deliberate (by Argon puffing) disruptions of outer poloidal limiter configurations with the potentiality of generating RE, performed to study the efficiency in RE prevention of high rate Helium puff. The plasma current and the toroidal field in all these experiments were 2MA and 3T respectively; the pre-disruption plasma store energy was ~1.4MJ. The default minimum temperature of the IR was 80^{o}C in these discharges. Int(HXR) is the time integral, over the current quench, of the HXR signal; this is in arbitrary, but pulse independent, units. Ip-ind refers to the presence of a plateau during the plasma current decay.

Pulse No:	Note	I_p [MA]	B_T [T]	RE	F_v [kN]	R_{Side} [mm]	I_{halo} [kA]	IR
54055	Switch off + He 2400 mbarl	2	2.6	N	700	<0.1	120	N/A
54056	Switch off + He 2400 mbarl	2	2.6	N	600	0.15	120	N/A
54057	Kick up	2	2.6	N	1000	<0.1	170	N/A
54058	Kick up + He 2400 mbarl	2	2.6	N	1500	0.6	170	N/A
54283	Kick up	1.5	1.6	?	700	0.7	340	N/A
54284	Kick up + He 1000 mbarl	1.5	1.6	?	1000	0.4	240	Light?
54285	Kick down	1.5	1.6	Y	1100	<0.1	310	N/A
54286	Kick down + He 1000 mbarl goes up	1.5	1.6	?	900	0.6	220	N/A
54287	X-kick down + He 1000 mbarl	1.5	1.6	?	1100	<0.1	290	Light on inner (1f), septum 500^{0}C (slow decay) IR rate: 7 ms/frame
54288	Kick down (rep. 54285)	1.5	1.6	?	1100	<0.1	370	Light on inner (1f), septum 350^{0}C (slow decay) IR rate: 7 ms/frame
54289	Kick up + He 230 mbarl	1.5	1.6	Y!	1400	0.9	210	N/A

Tab50107

Table 5: Divertor heat loads of deliberate VDEs to study the amelioration efficiency of high rate Helium puffing. The pre-disruption plasma stored energy was ~2.5MJ for the 2MA/2.6T discharges and ~0.6MJ for the 1.5MA/1.6T discharges. No significant temperature variation was registered by the TCs. The default minimum temperature of the IR was 800 C in these discharges. F_v is the vessel vertical force and R_{Side} is the vessel sideways displacement after the disruption. I_{halo} is the poloidal halo current (measured by toroidal field pick-up coils).

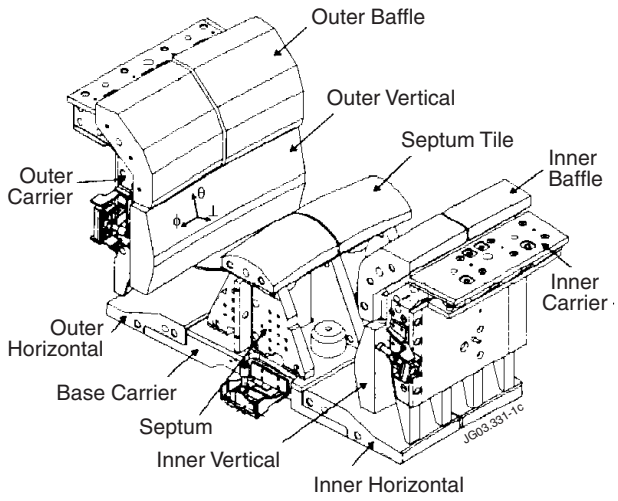

Figure 1: 3D view of the JET MkIIGB divertor; the tile local co-ordinate system is shown on the outer vertical tile: θ is the toroidal direction, ϕ is the poloidal direction and ⊥ is the direction perpendicular to the plasma facing surface.

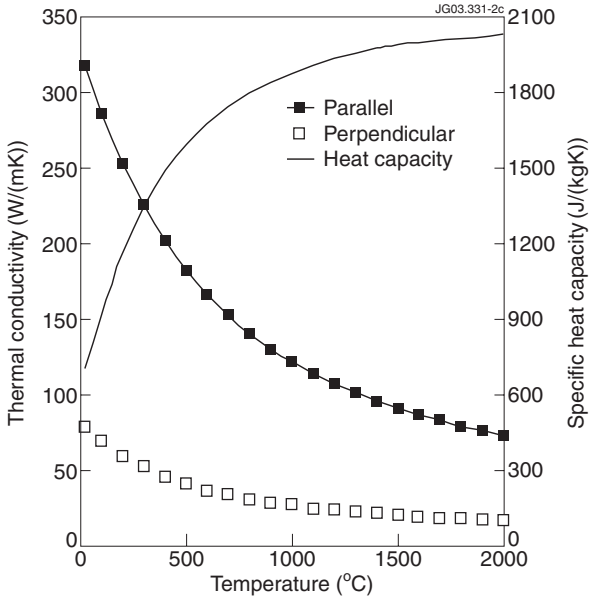

Figure 2: As-built thermal properties of the MkIIGB divertor tiles (parallel and perpendicular refer to the weave planes).

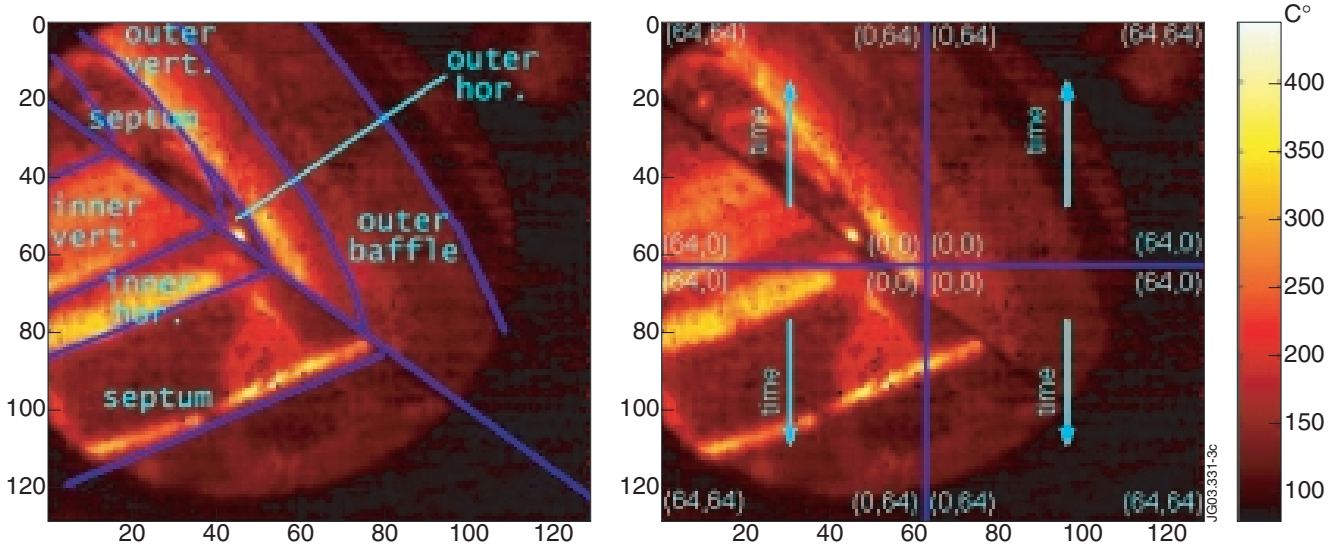

Figure 3: View of the infra-red camera: (left) map of the divertor sub-components and trace of the mirror separation; (right) number of pixels and direction of data collection.

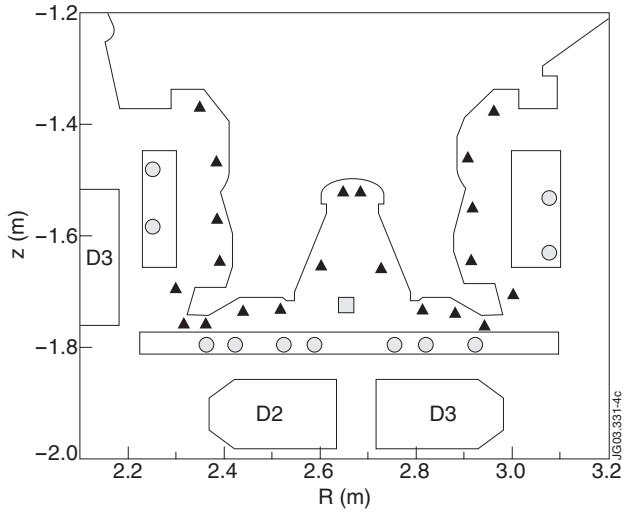

Figure 4: Poloidal section of the JET MkIIGB divertor. Locations of thermocouples are marked by triangles, of 2D poloidal field pick-up coils by circles and of the halo probe (a toroidal field pick-up coil) by a square.

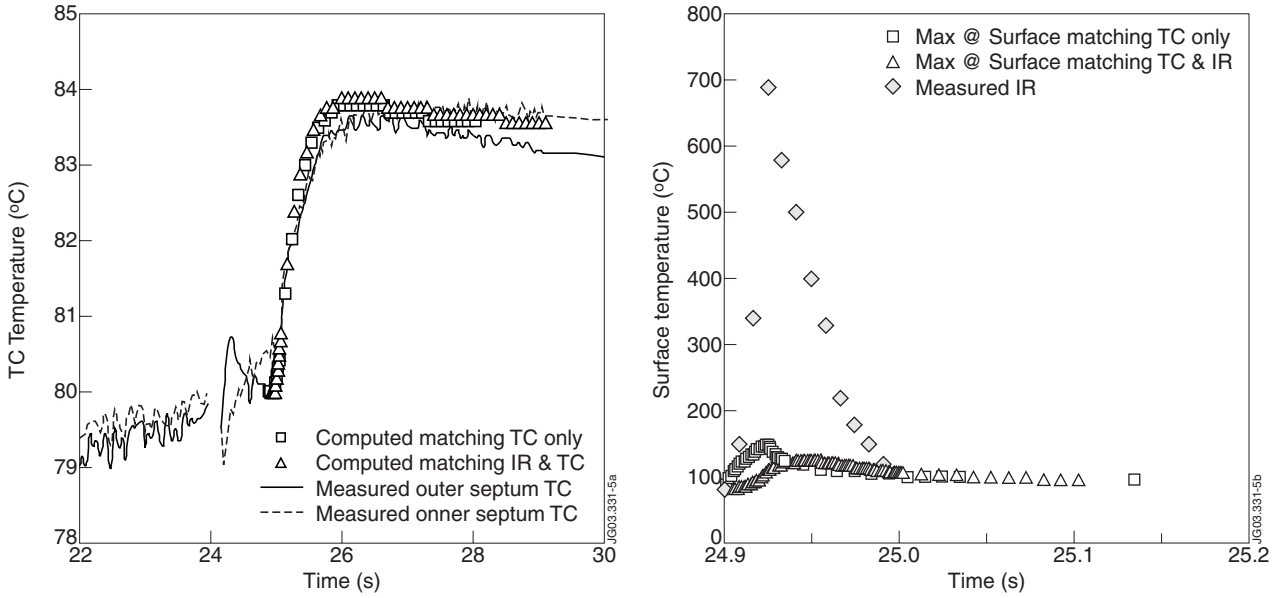

Figure 5: Comparison of measured and computed temperature variation at the septum for the disruption of Pulse No: 54287. TCs in the left frame: squares for the traditional imposed power density method, triangles for prescribed IR temperatures in front of the surface layer. Septum surface in the right frame: same symbols as above, and including IR reading, shown with large diamonds.

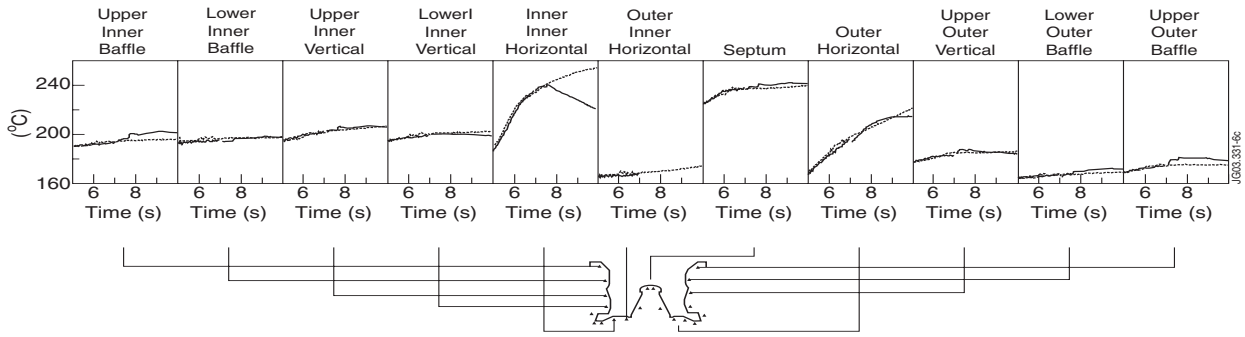

Figure 6: TC traces for Pulse No's: 51976 (solid) and 51972 (dotted) around the time of the disruption of 51976.

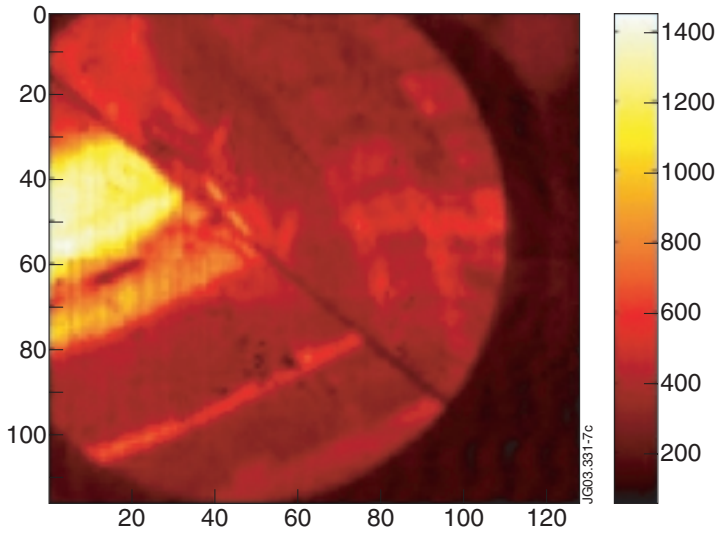

Figure 7: IR image of the disruption of Pulse No: 51976, taken at the time of the peak IR-recorded inner target temperature.

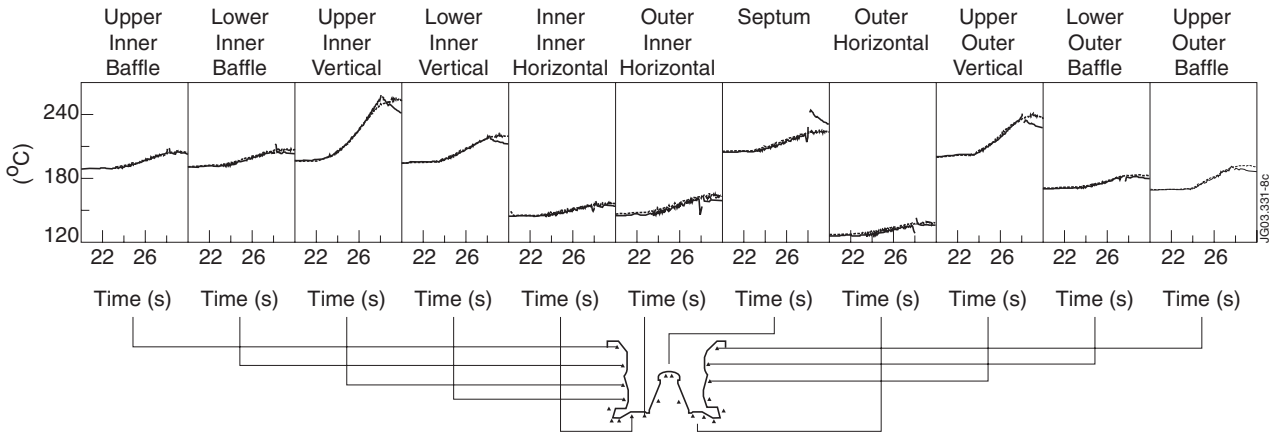

Figure 8: TC traces for Pulse No's: 51988 (solid) and 51989 (dotted) around the time of the disruption of Pulse No: 51988.

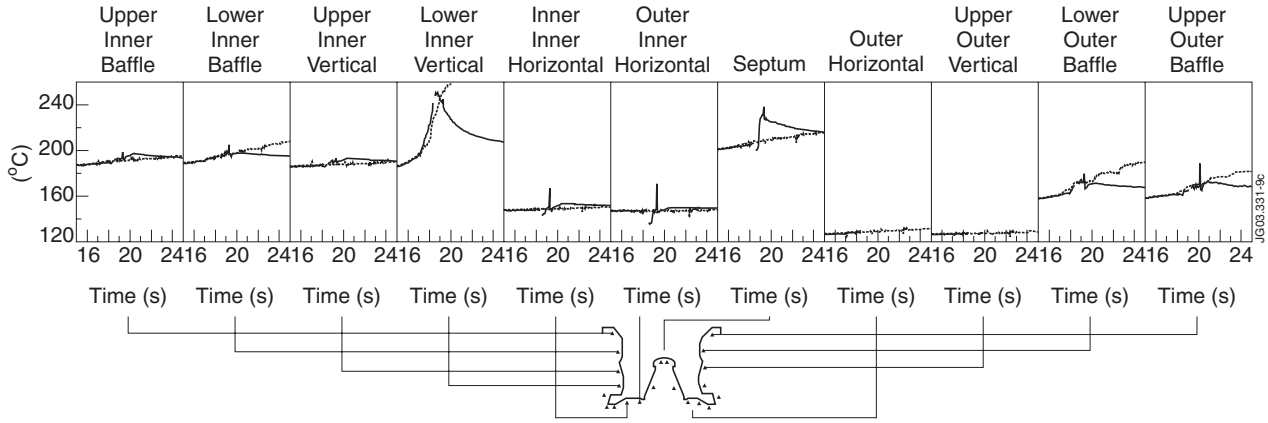

Figure 9: TC traces for Pulse No's: 52018 (solid) and 52021 (dotted) around the time of the disruption of Pulse No: 52018.

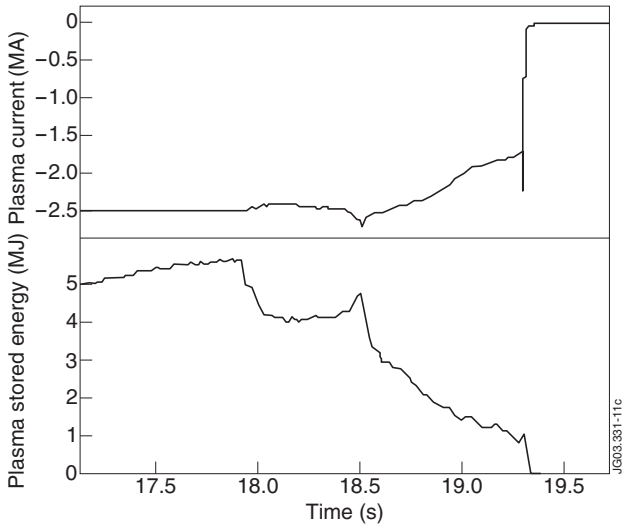

Figure 10: Plasma current and stored energy for the Pulse No: 52018, showing a delay between the loss of energy and the loss of current.

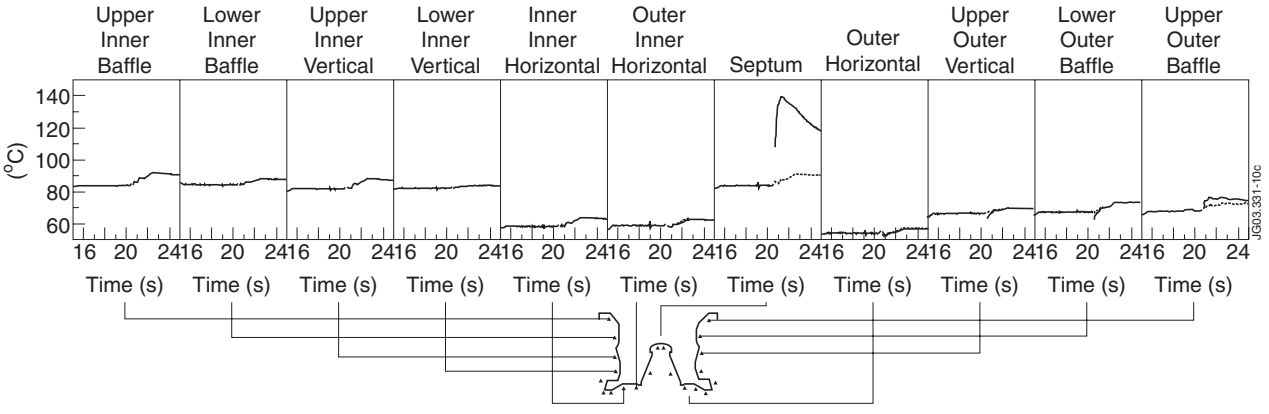

Figure 11: TC traces for Pulse No's: 54327 (solid) and 53790 (dotted), both discharges were disrupted at the same sequence time (50s).

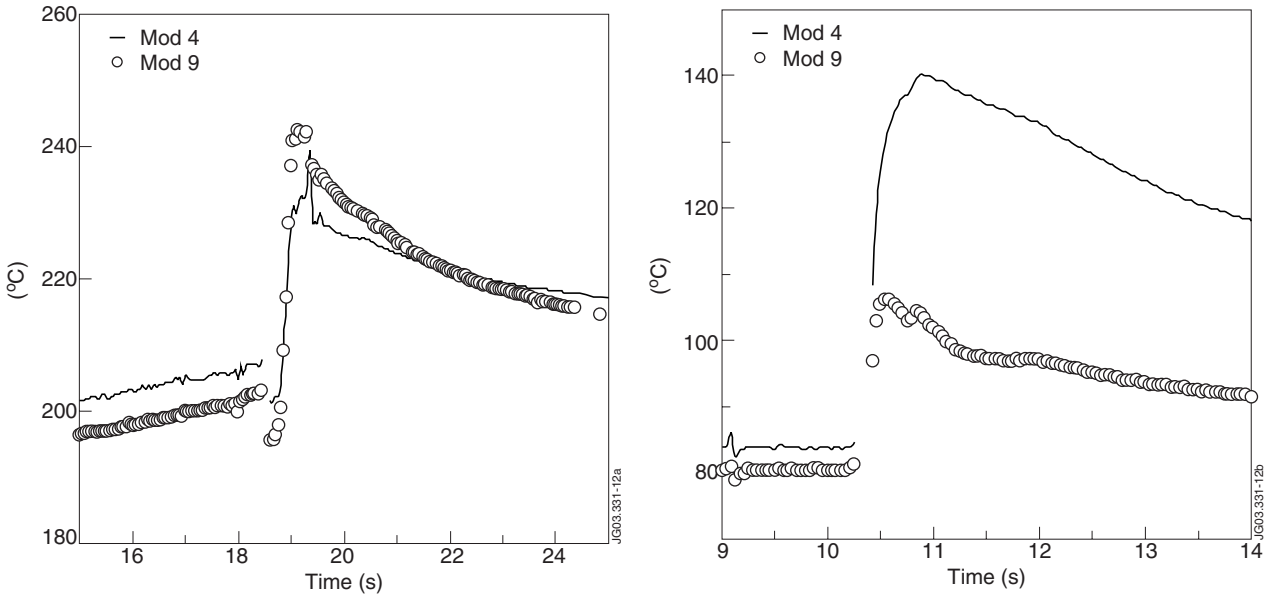

Figure 12: Outer septum temperature in different toroidal locations for Pulse No's: 52018 (left) and 54327 (right).

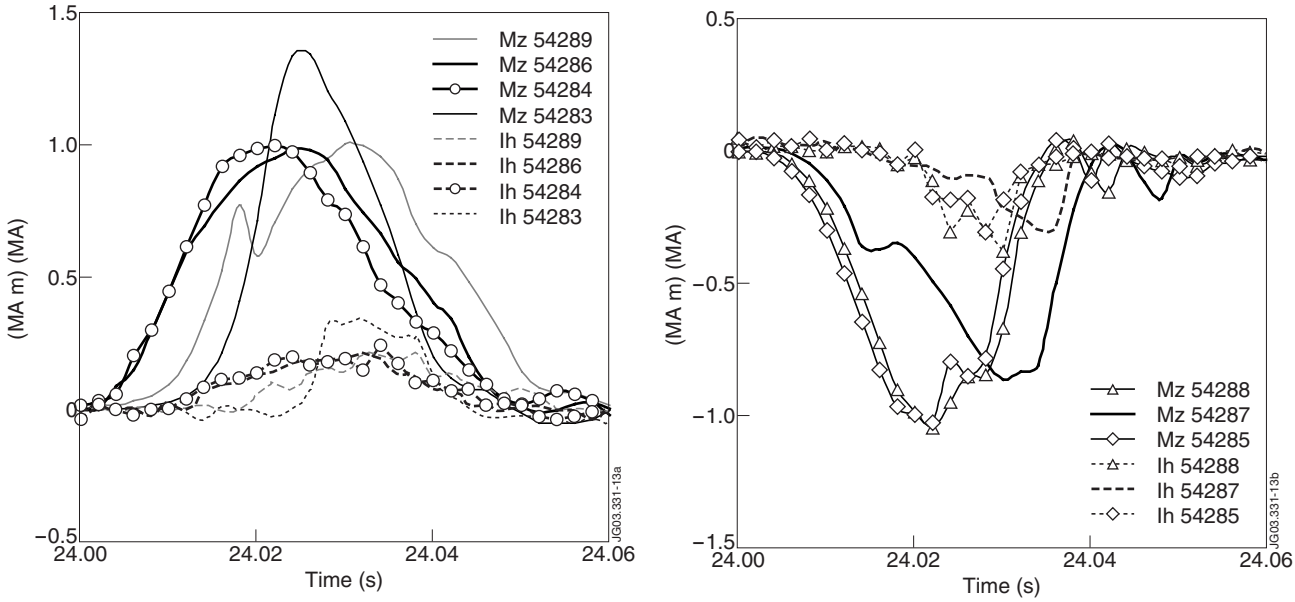

Figure 13 Vertical current moment variation and poloidal halo current for the disruption amelioration discharges performed with the ITER-like configuration (Table 5): kicked up (top: 54284, 54286 and 54289 with He-puff; 54283 reference without He-puff) and kicked down (bottom: 54287 with He-puff; 54285 and 54288 without He-puff).

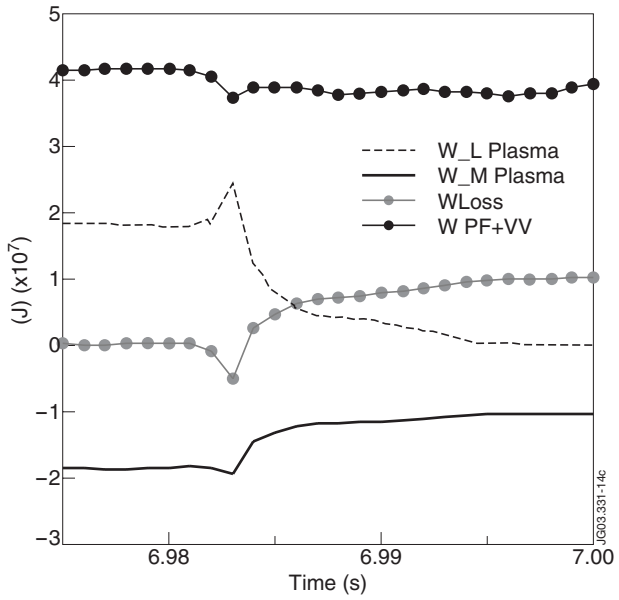

Figure 14: Plasma self and mutual magnetic energy, total plasma energy and magnetic energy as a function of time during the disruption of Pulse No: 51976.